

Breakdown of chiral symmetry during saturation of the Tayler instability

Alfio Bonanno,^{1,2} Axel Brandenburg,^{3,4} Fabio Del Sordo,^{3,4} and Dhrubaditya Mitra³

¹*INAF, Osservatorio Astrofisico di Catania, Via S. Sofia 78, 95123 Catania, Italy*

²*INFN, Sezione di Catania, Via S. Sofia 72, 95123 Catania, Italy*

³*Nordita, Royal Institute of Technology and Stockholm University, Roslagstullsbacken 23, SE-10691 Stockholm, Sweden*

⁴*Department of Astronomy, Stockholm University, SE 10691 Stockholm, Sweden*

(Dated: August 6, 2018, Revision: 1.191)

We study spontaneous breakdown of chiral symmetry during the nonlinear evolution of the Tayler instability. We start with an initial steady state of zero helicity. Within linearized perturbation calculations, helical perturbations of this initial state have the same growth rate for either sign of helicity. Direct numerical simulations (DNS) of the fully nonlinear equations, however, show that an infinitesimal excess of one sign of helicity in the initial perturbation gives rise to a saturated helical state. We further show that this symmetry breaking can be described by weakly nonlinear finite-amplitude equations with undetermined coefficients which can be deduced solely from symmetry consideration. By fitting solutions of the amplitude equations to data from DNS we further determine the coefficients of the amplitude equations.

PACS numbers: 52.35.Py, 11.30.Qc, 07.55.Db, 47.20.Bp

I. INTRODUCTION

There are many examples in nature where the ground state does not share the same symmetries of the underlying equations of motion [1]. The most common examples include equilibrium phase transition, e.g., the case of a liquid-solid transition where the space translational symmetry is broken, or that of a paramagnetic-ferromagnetic transition where the spin-rotational symmetry is broken; see e.g., Ref.[2] for a detailed discussion. However, the original symmetry is not lost but gives rise to the appearance of a regular structure with a specific length scale.

In non-equilibrium physics spontaneous symmetry breaking is often observed when some control parameter is increased above a critical value, see e.g., Ref [3] for a comprehensive introduction. Two well-studied examples from fluid dynamics include the case of Rayleigh-Bénard convection [3] and the Mullins-Sekerka instability of a moving interface between two phases [4]. These systems, too, are invariant under translation and reflection, but the basic instability produces a symmetry breaking bifurcation in which the continuous translational symmetry of the basic state is broken to a discrete one, although the mirror symmetry is often retained. If the instability parameter is raised further, secondary instabilities may break the periodic pattern and eventually a completely new symmetry-broken state may emerge, as has been seen in several experiments [5]. At very high values of the control parameter, turbulence sets in and most of the symmetries are statistically restored.

In a hydrodynamic system under rotation, spontaneous breakdown of chiral symmetry has been studied; see, e.g., Ref. [7]. Spontaneous chiral symmetry breaking is also found in liquid crystals [6]. Preliminary evidence showing spontaneous chiral symmetry breaking in magnetohydrodynamics (MHD), in the absence of rotation, has been presented for the magnetic buoyancy instability [8] and for the Tayler instability in a Taylor-Couette setup [9]. However the role of the dynamics of the bifurcation process is still poorly understood.

The purpose of the present paper is twofold. First we

demonstrate the occurrence of spontaneous chiral symmetry breaking in the context of a global instability of the toroidal field, and second we elucidate some aspects of the underlying nonlinear mechanism which determines the evolution from a mirror-symmetric state to a state with a preferred handedness or helicity. In particular, we shall be interested in the case of the Tayler instability [10, 11], which has attracted much interest in recent times for its possible astrophysical applications [9, 12–18]. We thus discuss the possibility of generating a final state with finite helicity starting from a non-helical basic state, using a very small controlled helical perturbation.

Our setup has the advantage of better clarifying the complex nonlinear coupling between the different modes, which eventually leads to the formation of a final helical state. In fact, the Tayler instability, in its simplest realization, has no threshold field, at least in ideal MHD [13], where a sufficient condition for instability simply reads

$$\beta \equiv \frac{\partial \ln B_\varphi}{\partial \ln s} > -\frac{1}{2}, \quad (1)$$

s being the cylindrical radius. On the other hand, the spectrum is characterized by an infinite number of unstable modes all characterized by pairs of opposite azimuthal wave number $m = \pm 1, 2, 3, \dots$, but with precisely the same growth rate. In particular, as is well known, $m = \pm 1$ are the modes with the fastest growth rate. Here our aim is to understand the dynamics of the bifurcation process which leads to the selection of a final state of finite helicity and to understand the evolution of the system after the bifurcation takes place. It should also be noted that in the linear stage the preferred helicity is determined essentially by the helicity of the perturbation, but the nonlinear evolution can be rather complex and it is not clear a priori what the final selected helical state would be.

The rest of the paper is organized as follows. In Section II we write down the finite-amplitude equations that govern the evolution of the instability in the weakly nonlinear phase. Our approach is based on symmetry arguments; a detailed analytical derivation of the amplitude equations is avoided here. We find that the amplitude equations predict a breakdown of

parity for certain choice of parameters. Direct numerical simulations (DNS) of the fully nonlinear equations describing the evolution of the Taylor instability are performed in Section III. In our DNS studies we also find breakdown of parity. We fit data from DNS to solutions of the amplitude equations to numerically determine the parameters appearing in the amplitude equations. It turns out that the amplitude equations we deduce are identical to those used to describe the breakdown of mirror symmetry in studies of the biochemical origin of life. This connection is explored in Section IV. Finally conclusions are drawn in Section V

II. AMPLITUDE EQUATIONS

To the best of our knowledge the amplitude equations describing the spontaneous breakdown of mirror symmetry in hydrodynamic instabilities were first described in Ref. [19]. The basic idea is as follows.

Let us consider an instability with two growing modes with opposite helicity but exactly the same growth rate and let the amplitude in this basis of the left- and right-handed modes be given by vectors $\hat{\mathbf{L}}$ and $\hat{\mathbf{R}}$, respectively. In physical space we have

$$\mathbf{L}(\mathbf{x}) = \hat{\mathbf{L}}\phi(\mathbf{n}), \quad (2)$$

$$\mathbf{R}(\mathbf{x}) = \hat{\mathbf{R}}\phi(\mathbf{n}). \quad (3)$$

For example, in Cartesian domains, with real-space coordinate \mathbf{x} , $\phi(\mathbf{n}) = \exp(i\mathbf{n} \cdot \mathbf{x})$. In cylindrical coordinate, ϕ is a combination of trigonometric and Bessel functions. As the modes are helical they satisfy the Beltrami relation,

$$\nabla \times \mathbf{R} = \Lambda \mathbf{R} \quad \text{and} \quad \nabla \times \mathbf{L} = -\Lambda \mathbf{L}. \quad (4)$$

For the present problem, explicit expressions involve a linear combinations of the type $J_m(s\sqrt{\Lambda^2 + n^2\pi^2/h^2})\cos(m\phi)\cos(zn\pi/h)$, where J_m is the Bessel function of the first kind, $n, m = \pm 1, 2, 3 \dots$, h is the height of the cylinder and s the cylindrical radius [20]. The set of such modes forms a complete set (a Hilbert basis) for the spatial distribution of the field.

Here we assume that the dynamical evolution of the unstable mode is determined by an effective Lagrangian. For the left-handed helical mode, total helicity and energy are given by

$$E_L = \frac{1}{2} \int \mathbf{L}^2(\mathbf{x}) d^3x = \frac{1}{2} \hat{\mathbf{L}} \cdot \hat{\mathbf{L}}^*, \quad (5)$$

$$\mathcal{H}_L = \int \mathbf{L} \cdot \nabla \times \mathbf{L} d^3x = -2\Lambda E_L. \quad (6)$$

where an asterisk denotes complex conjugation. Analogous definitions apply also to E_R and $\mathcal{H}_R = +2\Lambda E_R$. We then have $E = E_L + E_R$ being the total energy and $\mathcal{H} = \mathcal{H}_L + \mathcal{H}_R$ the total helicity. In the weakly nonlinear regime the amplitude equations can be written as

$$\frac{\partial \hat{\mathbf{L}}}{\partial t} = \frac{\delta \mathcal{L}}{\delta \hat{\mathbf{L}}} \quad \text{and} \quad \frac{\partial \hat{\mathbf{R}}}{\partial t} = \frac{\delta \mathcal{L}}{\delta \hat{\mathbf{R}}}, \quad (7)$$

where the simplest form of the Lagrangian is given by

$$\mathcal{L}[\hat{\mathbf{L}}, \hat{\mathbf{R}}] = \gamma \left[|\hat{\mathbf{L}}|^2 + |\hat{\mathbf{R}}|^2 \right] - \mu \left[|\hat{\mathbf{L}}|^4 + |\hat{\mathbf{R}}|^4 \right]. \quad (8)$$

The form of the Lagrangian is determined by the symmetry of the problem. The coefficient γ is the linear growth rate and μ determines the saturation of the instability in the weakly nonlinear regime. We emphasize that the μ and γ for $\hat{\mathbf{L}}$ and $\hat{\mathbf{R}}$ could be different if and only if the chiral symmetry is broken from the outset, but this is *not* the case here. Now note that the Lagrangian must also be invariant under the parity transformation, under which

$$\mathcal{P}(\hat{\mathbf{L}}) = \hat{\mathbf{R}} \quad \text{and} \quad \mathcal{P}(\hat{\mathbf{R}}) = \hat{\mathbf{L}}. \quad (9)$$

This additional symmetry allows one additional term in the Lagrangian given by

$$- \mu_* \left(|\hat{\mathbf{L}}|^2 |\hat{\mathbf{R}}|^2 \right). \quad (10)$$

With this additional term in the Lagrangian the evolution equations for the two eigenmodes are given by

$$\frac{\partial \hat{\mathbf{L}}}{\partial t} = \gamma \hat{\mathbf{L}} - \left(\mu |\hat{\mathbf{L}}|^2 + \mu_* |\hat{\mathbf{R}}|^2 \right) \hat{\mathbf{L}}, \quad (11a)$$

$$\frac{\partial \hat{\mathbf{R}}}{\partial t} = \gamma \hat{\mathbf{R}} - \left(\mu |\hat{\mathbf{R}}|^2 + \mu_* |\hat{\mathbf{L}}|^2 \right) \hat{\mathbf{R}}. \quad (11b)$$

These equations, for certain parameters, allow and can describe the growth of one handedness while the other is extinguished [19]. Similar equations, which describe the time dependence of the amplitudes of the leading modes, but without considering their spatial dependence, are often used to extend linear perturbation theory of hydrodynamic instabilities into the weakly nonlinear regime. In this form they are often called the Landau equations [21].

The energy of the left and right-handed modes is determined by,

$$\frac{dE_L}{dt} = 2\gamma E_L - 4\mu E_L^2 - 4\mu_* E_L E_R, \quad (12a)$$

$$\frac{dE_R}{dt} = 2\gamma E_R - 4\mu E_R^2 - 4\mu_* E_L E_R. \quad (12b)$$

These equations show that both E_L and E_R grow exponentially at the rate 2γ until nonlinear effects become important and either E_L or E_R saturates at $E_0 \equiv \gamma/2\mu$ and the energy of the mode of opposite handedness vanishes. In principle, the achiral solution with $E_L = E_R \equiv E_a = \gamma/2(\mu + \mu_*)$ is also possible, but, as we will see below, such a solution is unstable for $\mu < \mu_*$, which is what we find Sect. III. The reason for this instability is the presence of the term proportional to μ_* , which represents a phenomenon known as ‘‘mutual antagonism’’ in studies of the origin of homochirality of biomolecules [22–24]. We will return to this issue in Sect. IV, where we discuss the analogy with chiral symmetry breaking in biomolecules in more detail.

Using Eqs. (6) and (11) and defining $H = \mathcal{H}/2\Lambda$ we have $E_R = (E + H)/2$ and $E_L = (E - H)/2$. We can thus obtain

the following evolution equations

$$\frac{dE}{dt} = 2\gamma E - 2(\mu + \mu_*)E^2 - 2(\mu - \mu_*)H^2, \quad (13a)$$

$$\frac{dH}{dt} = 2\gamma H - 4\mu EH. \quad (13b)$$

The dynamical system described by (13) and depicted in Fig. 1 has four fixed points in the (E, H) plane, $S_1 = (0, 0)$, $S_{2,3} = (E_0, \pm E_0)$, and $S_4 = (2E_a, 0)$ with eigenvalues $\lambda_1 = (2\gamma, 2\gamma)$, $\lambda_2 = \lambda_3 = (-2\gamma, 2(\mu - \mu_*)/\gamma)$, and $\lambda_4 = (-2\gamma, 2\gamma - 4\gamma\mu/(\mu + \mu_*))$. The origin is always repulsive while S_2 and S_3 are sinks or saddle points depending on the values of parameters μ and μ_* . S_4 , corresponding to the achiral solution, can be an attractive point only if $\mu_* < \mu$, otherwise is a saddle point.

A discussion of the amplitude equations is now in order. Firstly, we have assumed that there are exactly two modes of opposite helicity that becomes critical at the onset of the instability. This assumption is based on linear perturbation analysis. As all the other modes in this case stable, in the spirit of center manifold reduction, we have ignored their contributions to total energy and helicity. If several modes are simultaneously unstable at the onset, then we may expect a higher degree of complexity. Secondly, as our approach is based on symmetry, the form of the amplitude equations that we obtain is very general. This is also a weakness of our approach, as we cannot determine the expression for either μ or μ_* . In principle, the method of multiscale expansion or center manifold reduction can be applied to this problem to derive analytical expressions of μ and μ_* , but this is a difficult proposition in the present case as a solution of the linear problem itself is not known in an analytically closed form.

We can then compute the quantities γ , μ and μ_* with the help of direct numerical simulations (DNS) by comparing the time evolution obtained for the left-hand side of (13) in the weakly nonlinear phase where our description is valid. We can anticipate that in most of our simulations $\mu < \mu_*$ and therefore the system should relax to a state of finite helicity in a finite time, although we start from an infinitesimally small helicity. This is precisely what we observe in our DNS.

III. DIRECT NUMERICAL SIMULATIONS

To analyze the evolution of the Tayler instability we choose our numerical domain to be a cylindrical shell with an inner radius $s_{\text{in}} = 1$, outer radius $s_{\text{out}} = 3$, and height $h = 2$. We perform simulations of the time-dependent resistive magnetohydrodynamic equations for a compressible isothermal gas: the pressure is thus given by $p = \rho c_s^2$, where ρ is the density and c_s is the isothermal sound speed.

We use the PENCIL CODE [30] to solve the equations for the magnetic vector potential \mathbf{A} , ($\mathbf{B} = \nabla \times \mathbf{A}$) the velocity \mathbf{U} , and the logarithmic density $\ln \rho$ in the form

$$\frac{\partial \mathbf{A}}{\partial t} = \mathbf{U} \times \mathbf{B} + \eta \nabla^2 \mathbf{A}, \quad (14)$$

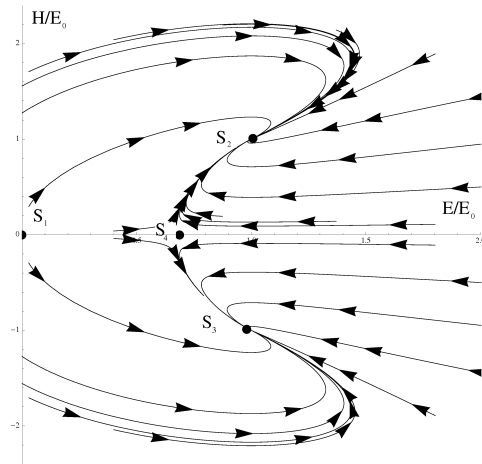


FIG. 1: The phase portrait for $\mu < \mu_*$. This is the typical situation in which S_2 and S_3 are attractive and S_4 is a saddle point.

$$\frac{D\mathbf{U}}{Dt} = -c_s^2 \nabla \ln \rho + \mathbf{J} \times \mathbf{B} / \rho + \mathbf{F}_{\text{visc}}, \quad (15)$$

$$\frac{D \ln \rho}{Dt} = -\nabla \cdot \mathbf{U}, \quad (16)$$

where

$$\mathbf{F}_{\text{visc}} = \rho^{-1} \nabla \cdot 2\nu \rho \mathbf{S}$$

is the viscous force, \mathbf{S} is the traceless rate of strain tensor having components $S_{ij} = \frac{1}{2}(U_{i,j} + U_{j,i}) - \frac{1}{3}\delta_{ij} \nabla \cdot \mathbf{U}$,

$$\mathbf{J} = \nabla \times \mathbf{B} / \mu_0$$

is the current density, ν is the kinematic viscosity, and η is the magnetic diffusivity.

We choose periodic boundary conditions in the vertical (z) and azimuthal (φ) directions, while at radial (s) boundaries we select perfectly conducting boundary condition for the magnetic field and stress-free boundary conditions for velocity. The resolution of the simulations presented here is 128^3 mesh-points in all three directions, but comparison with different resolution demonstrated that our results are converged.

We choose a basic state with zero velocity and zero axial component of the magnetic field (B_z). The azimuthal component of the magnetic field is

$$B_\varphi = B_0 (s/s_0) \exp[-(s - s_0)^2/\sigma^2], \quad (17)$$

where B_0 is a normalization constant, $s_0 = 2$ and $\sigma = 0.2$. We choose B_0 and c_s in such a way that the sound speed is much larger than the Alfvén speed. In this way we avoid magnetic perturbations to be dominant over hydrodynamical perturbations.

In the basic state the Lorentz force due to the magnetic field is balanced by the gradient of pressure. Hence the pressure of

the fluid is given by

$$p = p_0 - \frac{B_0^2}{4s_0^2} \left[(2s^2 - \sigma^2) e^{-2\frac{(s-s_0)^2}{\sigma^2}} + s_0 \sigma \sqrt{\pi} \sqrt{2} \operatorname{erf} \left(\frac{\sqrt{2}(s-s_0)}{\sigma} \right) \right], \quad (18)$$

where p_0 is a constant that must be large enough to ensure that the pressure is positive. If no perturbation is added, the system remains stationary. Therefore, we add at the beginning of the simulation a perturbation of the magnetic field with an infinitesimally small net helicity given by the following expression:

$$\mathbf{A} = \delta s \cos \left(z \frac{n_z \pi}{h} \right) \begin{pmatrix} \sin m\varphi \\ 0 \\ \cos m\varphi \end{pmatrix}, \quad (19)$$

where δ is an arbitrary small amplitudes which we set to 10^{-7} for all the simulations and $k_z = q/s_{\text{in}} = n_z \pi/h$ is the vertical wavenumber of the perturbation.

As discussed in [13] kink instabilities are special case of the so called quasi-interchange instabilities, where combined azimuthal and vertical field are present in the basic state. In the incompressible limit the unstable eigenmodes can be described by a (t, z, φ) -dependence of the type $\propto \exp(\gamma t - ik_z z - im\varphi)$ where the growth rate γ is determined from a numerical solution of the nonlinear eigenvalue problem for the radial disturbance v_{1s}

$$\begin{aligned} & \frac{d}{ds} \left[\frac{1}{\lambda} (\gamma^2 + \omega_A^2) \left(\frac{dv_{1s}}{ds} + \frac{v_{1s}}{s} \right) \right] - k_z^2 (\gamma^2 + \omega_A^2) v_{1s} \\ & + 2\omega_B \left[\frac{m(1+\lambda)}{s^2 \lambda^2} \left(1 - \frac{\beta \lambda}{1+\lambda} \right) (\omega_{Az} + 2m\omega_B) \right. \\ & \left. + \frac{m\omega_{Az}}{s^2 \lambda^2} - k_z^2 \omega_B (1-\beta) \right] v_{1s} + \frac{4k_z^2 \omega_A^2 \omega_B^2}{\lambda(\gamma^2 + \omega_A^2)} v_{1s} = 0. \end{aligned} \quad (20)$$

Here $\omega_A = (\mathbf{B} \cdot \mathbf{k})/\sqrt{\rho}$ with $\mathbf{k} = (0, m/s, k_z)$, so $\omega_{Az} = k_z B_z/\sqrt{\rho}$. Furthermore, we have defined $\omega_B = B_\varphi/s\sqrt{\rho}$ and $\lambda = 1 + m^2/s^2 k_z^2$.

Equation (20) describes the stability problem as a nonlinear eigenvalue problem. This equation was first derived by Freidberg [25] in his study of MHD stability of a diffuse screw pinch (see also [13]). The author found that, for a given value of k_z , it is possible to obtain multiple values of the eigenvalue γ , each one corresponding to a different eigenfunction, and calculated γ for the fastest growing fundamental mode. The most general form of Eq. (20), taking into account compressibility of plasma, was derived by Goedbloed [26]. Since we study the stability assuming that the magnetic energy is smaller than the thermal one, the incompressible form of Eq. (20) can be a sufficiently accurate approximation, as we have verified. In our case at hand, $(\mathbf{B} \cdot \mathbf{k})/\sqrt{\rho} = m\omega_B = \omega_A$ because we are interested in pure kink (Tayler) instabilities, with $B_z \equiv 0$ in the basic state. Note that as $\omega_{Az} = 0$ in our case, Eq.(20) is invariant for $m \rightarrow -m$.

In this latter case, once (20) is solved and v_{1s} is obtained, the expressions for the other perturbed quantities denoted by the subscript ‘‘1’’, read

$$B_{1s} = -\frac{i}{\gamma s} B_\varphi v_{1s}, \quad (21a)$$

$$B_{1\varphi} = -\frac{i}{\gamma s} B_\varphi v_{1\varphi} - \frac{B_\varphi}{\gamma s} (\beta - 1) v_{1s}, \quad (21b)$$

$$B_{1z} = -\frac{i}{\gamma s} B_\varphi v_{1z}, \quad (21c)$$

$$v_{1\varphi} = \frac{-im}{(k_z s)^2 \lambda} \frac{\partial}{\partial s} (s v_{1s}) - \frac{2im\omega_B^2 v_{1s}}{\lambda(\gamma^2 + m^2\omega_B^2)}, \quad (21d)$$

$$v_{1z} = -\frac{i}{k_z s} \frac{\partial}{\partial s} (s v_{1s}) - \frac{m}{k_z s} v_{1\varphi}. \quad (21e)$$

Unfortunately even for the case of pure kink instabilities, (20) cannot be solved analytically and one has to determine the dispersion relation numerically. Therefore, to test our numerical setup we have solved numerically Eq. (20) for the basic state (17) for various values of B_0 and σ in the limit of small v_A/c_s ratio to check that in the linear phase the growth rate extracted from the DNS is in agreement with the linear theory. In particular, as the inner radius of the cylinder is not at $s = 0$, we have set $v_{1s} = 0$ at both inner and outer boundaries. Note here that the growth rate and eigenfunctions of this instability are known for the ideal MHD limit. Hence to compare with those results, we choose viscosity and magnetic diffusivity such that the dissipative time scales are much larger than the characteristic growth time (inverse of γ) of the instability.

The results are shown in Fig. 2 for the dimensionless growth rate $\Gamma = \gamma t_A$, where $t_A = s_{\text{out}} \sqrt{\rho}/B_0$ is the Alfvén travel time, as a function of the dimensionless vertical wave number $q = k_z s_{\text{in}}$ for model He1d in Table I, with $B_0 = 0.5$, and $n_z = 10$. In particular to compare the growth rate obtained from our DNS we have determined the characteristic vertical wave number of the unstable mode in the linear phase by means of the Fourier analysis of the magnetic fields. We also found that in all the simulations the azimuthal wave number of the fastest growing mode turned out to be always $m = \pm 1$ as higher values of $|m|$ have a smaller growth rate as shown in Fig. 2). We found that the corresponding growth rate determined from the linear phase of our direct numerical simulation is about 7 – 5% smaller than the linear value, we think this acceptable in view of unavoidable numerical diffusion in three-dimensional numerical simulations.

We see that the eigenfunction is rather localized for $q \gg 1$, as visible in the example shown in Fig. 3. We can exploit this property to obtain approximate explicit expressions for the growth rate at large values of q . In fact we can consider the magnetic field approximately constant around $s = s_0$ and apply the small-gap approximation (see [13] for details) so that $v_{1s} \propto \sin(\pi(s - s_0)/\sigma)$ and the dimensionless growth rate reads

$$\begin{aligned} \Gamma^2 = & -\frac{2c\Delta^2 m^2 ((\beta - 1)m^2 + (\beta - 3)q^2)}{(m^2 + q^2) (\Delta^2 (m^2 + q^2) + \pi^2)} \\ & + \frac{2(\beta - 1)\Delta^2 q^2 - c^2 m^2 (\Delta^2 (m^2 - 3q^2) + \pi^2)}{\Delta^2 (m^2 + q^2) + \pi^2}, \end{aligned} \quad (22)$$

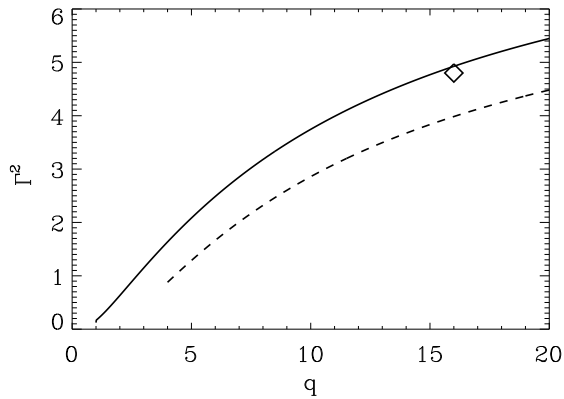


FIG. 2: The dispersion relation for the dimensionless growth rate Γ for the $m = \pm 1$ mode (solid line) and for the $m = \pm 2$ mode (dashed). Higher values of $|m|$ have even smaller growth rates. This curve is obtained for a linear model with physical parameters corresponding to the nonlinear model `He1d`, for which we indicate, with a rhombus, the growth rate for its faster growing mode.

where $c = B_\phi/B_0 \approx \text{const}$ and $\Delta = 2\sigma/s_0$. In the limit $q \gg 1$, despite the uncertain approximation that we have performed, expression (23) differs by only 20% from the numerical solution.

It is interesting to notice that, by using (21) in the limit $q \gg 1$ we obtain the explicit expressions

$$\langle \mathbf{v}_1 \cdot \nabla \times \mathbf{v}_1 \rangle \approx -\frac{4m\omega_B^2(\gamma^2 - m^2\omega_B^2)\langle v_{1s}^2 \rangle}{s_0^2 k_z (\gamma^2 + m^2\omega_B^2)^2}, \quad (23)$$

$$\langle \mathbf{B}_1 \cdot \nabla \times \mathbf{B}_1 \rangle \approx \frac{4mB_\phi^2\omega_B^2\langle v_{1s}^2 \rangle}{s_0^4 k_z (\gamma^2 + m^2\omega_B^2)^2}, \quad (24)$$

where the symbol $\langle \cdot \rangle$ denotes volume averaging. It is therefore clear that, at the nonlinear level, eigenfunctions with non-zero m will produce both kinetic and magnetic helicity whose sign will depend on the sign of m . The relevant point is that modes with opposite m have identical growth rate, but opposite kinetic and magnetic helicity and the fate of the final helicity is decided by the competition of modes with opposite azimuthal wavenumber.

Moreover, according to the oscillation theorem [27] as the $m = \pm 1$ are unstable, all the other modes with $m = \pm a$, where $a > 1$ is a positive integer, are also unstable, but with a smaller growth rate. As a consequence, although in the linear phase the $m = \pm 1$ modes dominate the linear growth, already in the weakly nonlinear phase the contribution of modes with $m \neq \pm 1$ can be also important for the selection of the final helical state.

The eigenfunctions appear clearly in our simulation and they fit quite well the eigenfunctions calculated by the linear model, as shown in Fig. 3. In our simulations, during the growing phase of the instability we observe a net increase of the helicity, as shown in Fig. 4 where we plot the time series of the normalized kinetic, current and magnetic helicity. It is interesting to notice that while kinetic helicity decays on the

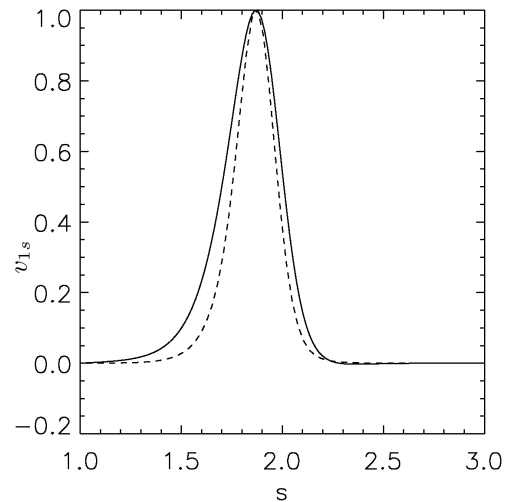


FIG. 3: Eigenfunction v_{1s} for the $m = 1$ mode for $q = 16$. The result of the simulation, model `He1d` in Table I (solid line) is overlaid on the eigenfunction obtained solving (20) (dashed line); see [13] for more details. This is observed at $t/t_A = 9$, that is during the linear growth of the instability.

viscous time scale, the current and magnetic helicities reach a nonzero value at very large times.

In actual simulations we choose $\nu = 10^{-2}$ (in code units), so that the viscous time scale is $t_\nu = s^2/\nu \gg \gamma^{-1}$ and the actual value of ν does not play a significant role in the weakly nonlinear phase as we verified in our simulations. Moreover we decided to use a very small value for the magnetic diffusivity, $\eta = 10^{-9}$ (in code units). This is done to prevent the decay of the magnetic field by diffusion. In general such small values of magnetic diffusivity would imply extremely large values of magnetic Reynolds number which would be impossible to resolve with the resolutions we use. Nevertheless we choose such values to have a toroidal field stable on time scales much longer than those of the instability. However, in our simulations no sharp gradients of the magnetic field develop, which is the reason why such small values of magnetic diffusivity are permissible.

We can now determine the coefficients γ , μ and μ_* using the time evolution of $H(t)$ and $E(t)$ obtained with our DNS in solving the model (13). This can be done via a direct two-parameter χ^2 minimization because the exponent γ can easily be determined from the linear evolution and one is left with only the determination of μ and μ_* . An example of this approach is depicted in Fig. 5, where the agreement with our numerical simulations is explicitly shown. Note that around $t/t_A \approx 6.5$ we enter the deep nonlinear phase and our treatment does not apply anymore. We estimate this cutoff time for our simulations to be in the middle of the decay transition for $d \ln H/dt$ and $d \ln E/dt$ depicted in Fig. 5 and we have checked that the values of μ and μ_* are not strongly dependent on our cutoff time.

Our results are summarized in Table I. We see that the coefficients μ and μ_* are unchanged for models that differ only in

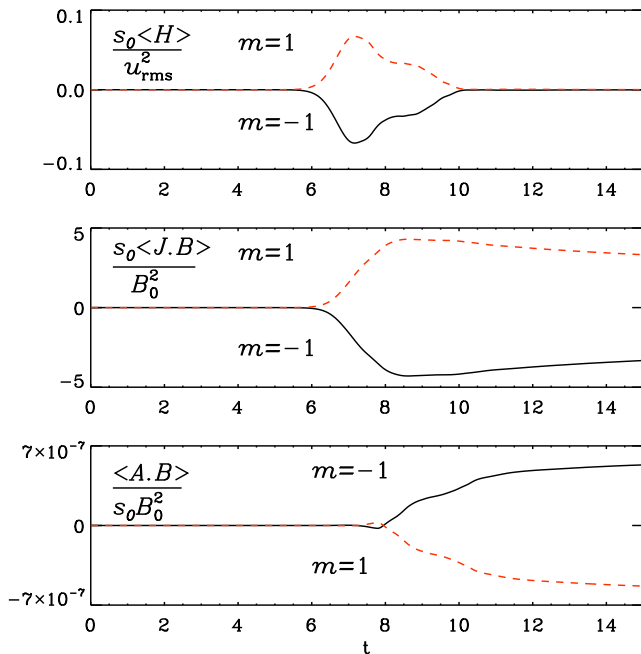


FIG. 4: (Color online) Kinetic, current, and magnetic helicities for two different runs (Models He1 and He1m1 in Table I) with helical perturbation and $m = \pm 1$. t is in units of the Alfvén travel time t_A . The viscous time is $t_\nu \approx 10^2 * t_A$ and the magnetic diffusion is $t_\eta \approx 10^9 * t_A$. It is clear the difference in the evolutions of the kinetic, current and magnetic helicities, in the first, second and third panel. These plots show how these quantities grow with the same rate, but different sign, depending on the sign of the initial perturbation, that is the sign of m . Note that for each model the magnetic helicity has opposite sign of the kinetic and current helicities.

the sign of m in the perturbation. This is what we expect and one of the symmetries we have used to write the Lagrangian (8). Model He1c shows that the growth rate depends on the value of c_s , but this does not change the values of μ and μ_* . Model Helb and model Held have a smaller growth rate due to a smaller v_A/c_s . Helb has μ and μ_* smaller than Held, due to the fact that in the latter modes with higher k_z have been excited by the initial perturbation. Note that in our setup the ratio v_A/c_s depends on B_0 , but not on c_s . This is due to the fact that the model is isothermal and the initial radial balance is obtained through a pressure gradient that balances the Lorentz force. An increase of n_z of the perturbation, as in model He1n10, leads to a similar growth rate, but smaller μ and μ_* . This can be explained saying that, while in the linear phase this model evolves similarly to any $n_z = 1$ model, in the weakly nonlinear phase the evolution is different because of a faster growth of modes with higher k_z . In our models we measure $2.2 \leq \mu_*/\mu \leq 2.6$.

IV. HOMOCHIRALITY IN BIOMOLECULES

It is instructive to consider Eqs. (12) as evolution equations for the concentration of two molecules of opposite handedness, L and R. Let us assume that L and R can be synthesized

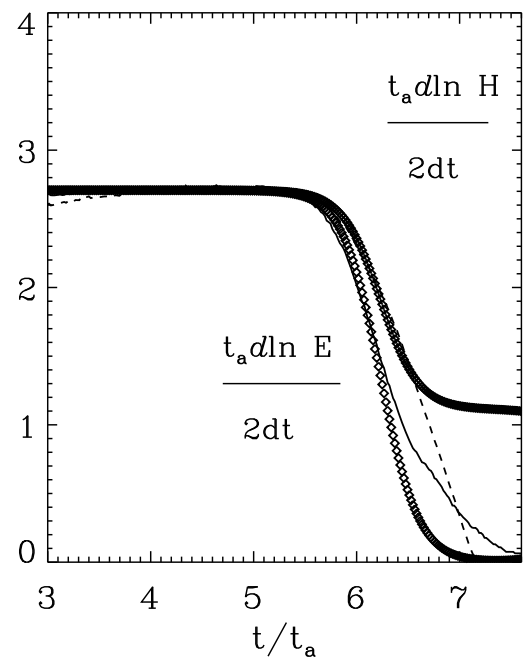
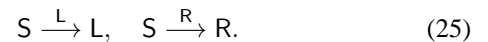


FIG. 5: Time evolution for the logarithmic derivative of kinetic energy (solid line) E and kinetic helicity H (dashed) as measured in DNS for models He1 and He1m1 (see I). t is in units of the Alfvén travel time t_A . We overplot a fit of the model with equations 13. The best fit is obtained for $\gamma = 2.71/t_A$, $\mu = 7.5 \cdot t_A/s_{out}^2$ and $\mu_* = 18 \cdot t_A/s_{out}^2$ and the solutions are over-plotted on the DNS results.

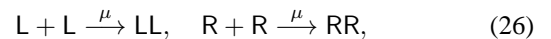
TABLE I: For every model s goes from 1 to 3, z from -1 to 1, the perturbation has an amplitude $\delta = 10^{-7}$, $\sigma = 0.2$.

Model	B_0^2/p_0	v_A/c_s	c_s	m	n_z	$\gamma \cdot t_A$	$\mu \frac{s_{out}^2}{t_A}$	$\mu_* \frac{s_{out}^2}{t_A}$	μ_*/μ
He1	10^{-1}	0.3	10	-1	1	2.71	7.5	18	2.4
He1m1	10^{-1}	0.3	10	+1	1	2.71	7.5	18	2.4
He1c	10^{-1}	0.3	20	-1	1	6.2	7	18.5	2.6
Helb	$2.5 \cdot 10^{-2}$	0.15	10	-1	1	2.2	1	2.3	2.3
Held	$2.5 \cdot 10^{-2}$	0.15	10	-1	10	2.2	3	7.3	2.4
He1n10	10^{-1}	0.3	10	-1	10	2.75	4.5	10	2.2

from a substrate S through auto-catalytic reactions of the form



Autocatalytic reactions of this type have been confirmed in laboratory experiments [28]. Let us furthermore assume that L and R are capable of polymerizing to form homochiral dimers,



as well as heterochiral dimers,



then the evolution equations for the various concentrations are

$$\frac{d[S]}{dt} = -k_C[S]([L] + [R]), \quad (28a)$$

$$\frac{d[L]}{dt} = k_C[S][L] - 2k_S[L]^2 - 2k_I[L][R], \quad (28b)$$

$$\frac{d[R]}{dt} = k_C[S][R] - 2k_S[R]^2 - 2k_I[L][R], \quad (28c)$$

$$\frac{d[LL]}{dt} = k_S[L]^2, \quad (28d)$$

$$\frac{d[RR]}{dt} = k_S[R]^2, \quad (28e)$$

$$\frac{d[LR]}{dt} = k_I[L][R], \quad (28f)$$

which obeys the conservation law [24]

$$[S] + [L] + [R] + 2[LL] + 2[RR] + 2[LR] = \text{const.} \quad (29)$$

These equations represent a subset of a more general polymerization model [23]. Comparing with Sect. II we see that Eqs. (28b) and (28c) are *identical* with Eqs. (12a) and (12b) when substituting $[L] = E_L$ and $[R] = E_R$, and identifying

$$k_C = 2\gamma, \quad k_S = 2\mu, \quad k_I = 2\mu_*. \quad (30)$$

Hence we demonstrate quantitatively that the spontaneous production of helicity from the fully nonlinear system of hydromagnetic equations can be described by the simple model equations (12), which in turn represent a simple set of chemical reactions (25)–(27).

The analogy with homochirality in biochemistry is useful because it helps identifying the phenomenon of mutual antagonism as the main cause of chiral symmetry breaking. This effect corresponds to a contribution to the nonlinear terms that result from the interaction between modes of opposite handedness. These are the terms proportional to μ_* and k_I in Eqs. (12) and (28), respectively. In the synthesis of polynucleotides this is known as enantiomeric cross-inhibition and has been identified in laboratory experiments [29]. The synthesis of heterochiral dimers is essential in that it corresponds

to the production of waste needed to eliminate building blocks of that handedness that is later is to disappear completely.

V. CONCLUSIONS

We have shown how net helicity is produced by the addition of a small helical perturbation to a non-helical system, thus driving the system to a final state characterized by a finite value of the helicities and, therefore, breaking the initial symmetry. We have shown further that this spontaneous symmetry breaking can be described by weakly nonlinear amplitude equations (13). Furthermore, we have numerically determined the coefficients appearing in the weakly nonlinear amplitude equations (13) for the Tayler instability. Direct numerical simulations show that the ratio between the coefficients describing the weakly nonlinear phase is almost constant. The agreement between the analytical model and the numerical solutions is rather good in the beginning of the weakly nonlinear phase, as shown in Fig. 5. This demonstrates quantitatively the close analogy between helicity production in hydromagnetic flows and the development of homochirality in biochemistry, which is described by the same system of equations as those resulting from the amplitude equations of the weakly nonlinear model of the Tayler instability. It will be useful to extend our analysis by means of a Landau-Ginzburg description of the amplitude equation by including non-homogeneous term in our Lagrangian to discuss the possible pattern formation in this type of spontaneous chiral symmetry breaking. We hope to address this issue in a following communication.

VI. ACKNOWLEDGEMENTS

The authors thank P. Chatterjee and M. Rheinhardt for useful discussions. A part of the work was performed when AB visited NORDITA under the program “Dynamo, Dynamical Systems and Topology”. FDS acknowledges HPC-EUROPA for financial support. Financial support from European Research Council under the AstroDyn Research Project 227952 is gratefully acknowledged.

-
- [1] H. Umezawa, *Thermo Field Dynamics and Condensed States*, Elsevier (1982).
 - [2] N. D. Goldenfeld, *Lectures on Phase Transitions and the Renormalisation Group*, Addison-Wesley, (1992).
 - [3] *Hydrodynamic Instabilities and the Transition to Turbulence*, edited by H.L. Swinney and J.P. Gollub (Springer-Verlag, New York, 1985), 2nd ed.; M. C. Cross and P. C. Hohenberg, Rev. Mod. Phys. **65**, 851 (1993).
 - [4] W. W. Mullins and R. F. Sekerka, J.App. Phys. **35**, 444 (1964).
 - [5] E. Moses and V. Steinberg, Phys. Rev. A **34**, 693 (1986); A. J. Simon, J. Bechhoeffer, and A. Libchaber, Phys. Rev. Lett. **61**, 2574 (1988); G. Faivre, S. de Cheveigne, C. Guthmann, and P. Kurowski, Europhys. Lett. **9**, 779 (1989); F. Melo and P. Oswald, Phys. Rev. Lett. **64**, 1381 (1990); H. Z. Cummins, L. Fournelle, and M. Rabaud, Phys. Rev. E **47**, 1727 (1993).
 - [6] J. V. Selinger, Z.-G. Wang, R. F. Bruinsma, and C. M. Knobler, Phys. Rev. Lett. **70**, 1139 (1993).
 - [7] A. Pinter, M. Lücke, and C. Hoffmann, Phys. Rev. Lett. **96**, 044506 (2006).
 - [8] P. Chatterjee, D. Mitra, A. Brandenburg, and M. Rheinhardt, Phys. Rev. E **84**, 025403R (2011). P. Chatterjee, D. Mitra, M. Rheinhardt, and A. Brandenburg, Astron. Astrophys. **534**, A46 (2011).
 - [9] M. Gellert, G. Rüdiger, and R. Hollerbach, Mon. Not. R. Astron. Soc. **414**, 2696 (2011).
 - [10] Tayler, R. J., Mon. Not. R. Astron. Soc. **161**, 365 (1973).
 - [11] Markey, P., Tayler, R. J., Mon. Not. R. Astron. Soc. **163**, 77 (1973).

- [12] A. Bonanno and V. Urpin, *Astron. Astrophys.* **477**, 35 (2008).
- [13] A. Bonanno and V. Urpin, *Astron. Astrophys.* **488**, 1 (2008).
- [14] A. Bonanno and V. Urpin, *Phys. Rev. E* **84**, 056310 (2011).
- [15] A. Bonanno and V. Urpin, *Astrophys. J.* **747**, 137 (2012).
- [16] J. Braithwaite and Å. Nordlund, *Astron. Astrophys.* **450**, 1077 (2006).
- [17] J. Braithwaite, *Astron. Astrophys.* **453**, 687 (2006).
- [18] H. Spruit, *Astron. Astrophys.* **349**, 189 (1999).
- [19] S. Fauve, S. Douady, and O. Thual, *J. Phys. II* **1**, 311 (1991).
- [20] F. Quingzeng, *Applied Mathematics and Mechanics*, **18**, 865 (1997).
- [21] L.D. Landau and E.M. Lifshitz, *Fluid Mechanics, Volume 6 (Course of theoretical physics)*, Pergamon Press, 2nd English Ed., Translated from *Gidrodinamika*, 3rd edition, "Nauka", Moscow, 1986, Chap. 3 (1987).
- [22] F. C. Frank, *Biochim. Biophys. Acta* **11**, 459 (1953).
- [23] P. G. H. Sandars, *Orig. Life Evol. Biosph.* **33**, 575 (2003).
- [24] A. Brandenburg, A. C. Andersen, S. Höfner, and M. Nilsson, *Orig. Life Evol. Biosph.* **35**, 225 (2005).
- [25] J. Freidberg, *Phys. Fluids*. 13, 1812 (1970).
- [26] J. P. Goedbloed, *Physica*. 53. 535 (1971).
- [27] J. P. H. Goedbloed and S. Poedts, *Principles of Magnetohydrodynamics*, CUP, (2004).
- [28] K. Soai, T. Shibata, H. Morioka, and K. Choji, *Nature* **378**, 767 (1995).
- [29] G. F. Joyce, G. M. Visser, C. A. A. van Boeckel, J. H. van Boom, L. E. Orgel, and J. Westrenen, *Nature* **310**, 602 (1984).
- [30] <http://pencil-code.googlecode.com/>